Applied Surface Science 257 (2011) 2717–2730

Contents lists available at ScienceDirect

Applied Surface Science

journal homepage: www.elsevier.com/locate/apsusc

Resolving surface chemical states in XPS analysis of first row transition metals, oxides and hydroxides: Cr, Mn, Fe, Co and Ni

Mark C. Biesinger[a,b,*], Brad P. Payne[c], Andrew P. Grosvenor[d], Leo W.M. Lau[a,c], Andrea R. Gerson[b], Roger St.C. Smart[b]

[a] Surface Science Western, The University of Western Ontario, The University of Western Ontario Research Park, Room LL31, 999 Collip Circle, London, Ontario, Canada N6G 0J3
[b] ACeSSS (Applied Centre for Structural and Synchrotron Studies), University of South Australia, Mawson Lakes, SA 5095, Australia
[c] Department of Chemistry, The University of Western Ontario, London, Ontario, Canada N6A 5B7
[d] Department of Chemistry, University of Saskatchewan, Saskatoon, Saskatchewan, Canada S7N 5C9

ARTICLE INFO

Article history:
Received 26 August 2010
Accepted 12 October 2010
Available online 20 October 2010

Keywords:
X-ray photoelectron spectroscopy
Transition metals
Chemical states
Peak fitting

ABSTRACT

Chemical state X-ray photoelectron spectroscopic analysis of first row transition metals and their oxides and hydroxides is challenging due to the complexity of their 2p spectra resulting from peak asymmetries, complex multiplet splitting, shake-up and plasmon loss structure, and uncertain, overlapping binding energies. Our previous paper [M.C. Biesinger et al., Appl. Surf. Sci. 257 (2010) 887–898.] in which we examined Sc, Ti, V, Cu and Zn species, has shown that all the values of the spectral fitting parameters for each specific species, *i.e.* binding energy (eV), full wide at half maximum (FWHM) value (eV) for each pass energy, spin–orbit splitting values and asymmetric peak shape fitting parameters, are not all normally provided in the literature and data bases, and are necessary for reproducible, quantitative chemical state analysis. A more consistent, practical and effective approach to curve fitting was developed based on a combination of (1) standard spectra from quality reference samples, (2) a survey of appropriate literature databases and/or a compilation of literature references and (3) specific literature references where fitting procedures are available. This paper extends this approach to the chemical states of Cr, Mn, Fe, Co and Ni metals, and various oxides and hydroxides where intense, complex multiplet splitting in many of the chemical states of these elements poses unique difficulties for chemical state analysis. The curve fitting procedures proposed use the same criteria as proposed previously but with the additional complexity of fitting of multiplet split spectra which has been done based on spectra of numerous reference materials and theoretical XPS modeling of these transition metal species. Binding energies, FWHM values, asymmetric peak shape fitting parameters, multiplet peak separation and peak area percentages are presented. The procedures developed can be utilized to remove uncertainties in the analysis of surface states in nano-particles, corrosion, catalysis and surface-engineered materials.

1. Introduction

Chemical state identification using X-ray photoelectron spectroscopy (XPS) has become routine for most elements in the periodic table. Binding energy databases, such as the NIST Database [1] or the Phi Handbook [2], generally provide sufficient data for the chemical state determination for uncomplicated (*i.e.* single peak) spectra. However, the transition metal 2p spectra pose a number of complications that these databases do not adequately address, specifically, shake-up and plasmon loss structures, and multiplet splitting, all of which can complicate identification of the chemical states present. For example, fitting parameters such as peak widths and asymmetries, which are vital for curve fitting of complex, mixed metal and metal oxide systems, are not reported in these databases. Importantly, some of the transition metal electronic states give rise to significant intensity components in their 2p spectra due to multiplet splitting and these contributions are not normally considered.

Multiplet splitting arises when an atom contains unpaired electrons. In these instances when a core electron vacancy is formed by photoionization there can be coupling between the unpaired electron in the core with the unpaired outer shell electron. This can create a number of final states, which will manifest in the photoelectron spectrum [2]. In the first transition series, low-spin Fe(II), low spin Ni(II), Cr(VI), and Mn(VII) species do not have unpaired d electrons and thus will not exhibit multiplet splitting. Cr(III), Mn(II),

* Corresponding author at: Surface Science Western, The University of Western Ontario, The University of Western Ontario Research Park, Room LL31, 999 Collip Circle, London, Ontario, Canada. Tel.: +1 519 661 2173; fax: +1 519 661 3709.
E-mail address: biesingr@uwo.ca (M.C. Biesinger).

0169-4332/$ – see front matter © 2010 Elsevier B.V. All rights reserved.
doi:10.1016/j.apsusc.2010.10.051

Mn(III), Mn(IV), Mn(VI), high-spin Fe(II), Fe(III), Co(II), Co(III), high-spin Ni(II), and Ni(III) species all contain unpaired d electrons and therefore exhibit multiplet structures [3]. Fitting this multiplet splitting is of far greater importance for these species than for Ti(II), Ti(III), V(II), V(III), and V(IV) species dealt with in our previous paper [4] as spectra for the later species generally are not resolved into their multiplet components (*i.e.* show only a broadened FWHM).

For some materials, where plasmon loss peaks occur, there is an increased probability of loss of a specific amount of energy due to the interaction between the photoelectron and conduction band electrons. For conductive metals, the energy loss (plasmon) occurs in well-defined quanta arising from excitation of group oscillations of the conduction band electrons [2]. Distinct plasmon losses attributed to conduction in the bulk or surface of the material can sometimes be separately identified. For example, deconvolution of Ni 2p metal spectra must include plasmon loss structures arising from both the bulk and the surface [5,6].

This paper outlines some recent spectral curve fitting procedures developed to elucidate quantitative chemical state information for a variety of transition metal-containing materials that give rise to significant multiplet splitting (specifically Cr, Mn, Fe, Co and Ni). Using a semi-empirical approach the fitting procedures applied determine the sum of the photoelectrons for each chemical state. This can then be directly related to the relative percentage of each chemical state at the surface of a sample. The data used for each species are based on one or a combination of (1) analysis of quality standard samples taken over the course of a number of years on a state-of-the-art Kratos Axis Ultra XPS spectrometer, (2) a survey of literature databases and/or a compilation of literature references, (3) specific literature references where fitting procedures are available and (4) theoretical fittings, where available, of multiplet split reference spectra, particularly those of Gupta and Sen [3]. Our fitting procedures have been tested and validated on both synthetic and practical samples and have been found to be consistently reproducible across a wide range of instances (*e.g.* [4,7–9]). Some of our recent work has already shown that chemical state identification using improved multiplet structure determination can also lead to more accurate estimates of mixed species in thin films of nickel oxide/hydroxide [5].

The starting point in the analysis of 2p spectra is the separation of $2p_{3/2}$ and $2p_{1/2}$ spin–orbit split components. In most cases, this separation is large enough to consider only the more intense $2p_{3/2}$ signal and its associated structure. The current databases attempt to assign oxidation states from the binding energy of this $2p_{3/2}$ signal assuming a single identifiable peak maximum. This assumption has been shown to be invalid for many transition metal spectra, *e.g.* Cr [10], Mn [11–14], Ni [5,6], and Fe [15,16].

The calculation of the multiplet structure of the core p and valence electron level interactions for the free ion first row transition metals by Gupta and Sen [3] graphically shows the contributions from their multiplet structure, which in some cases approaches 50% of the total intensity. These calculations are an excellent starting point for the examination of the multiplet structure observed for transition metal compounds. However, additionally there is frequently likely to be ligand charge transfer effects that will further affect the spacing and intensity of the spectral multiplet peaks. These relative changes can be employed in the analysis of transition metal compounds to distinguish between those species that more closely approximate free ions and those in which charge transfer from the bonded neighboring ions may affect both the oxidation state and multiplet splitting of the core transition metal photoelectron [6,10,15,16]. This perturbation has been specifically identified thorough the observation of differences between nickel oxide and its oxy/hydroxide spectra [6].

2. Experimental

XPS analyses were carried out with a Kratos Axis Ultra spectrometer using a monochromatic Al Kα source (15 mA, 14 kV). The instrument work function was calibrated to give an Au $4f_{7/2}$ metallic gold binding energy (BE) of 83.95 eV. The spectrometer dispersion was adjusted to give a binding energy of 932.63 eV for metallic Cu $2p_{3/2}$. Instrument base pressure was 8×10^{-10} Torr. High-resolution spectra were collected using an analysis area of ≈300 μm × 700 μm and either a 10 eV or 20 eV pass energy. These pass energies correspond to an Ag $3d_{5/2}$ FWHM of 0.47 eV and 0.55 eV, respectively.

The Kratos charge neutralizer system was used for all analyses with charge neutralization being monitored using the C 1s signal for adventitious carbon. A sharp main peak with no lower binding energy structure is generally expected. A single peak (Gaussian 70%–Lorentzian 30%), ascribed to alkyl type carbon (C–C, C–H), was fitted to the main peak of the C 1s spectrum for adventitious carbon. A second peak is usually added that is constrained to be 1.5 eV above the main peak, and of equal FWHM to the main peak. This higher binding energy peak is ascribed to alcohol (C–OH) and/or ester (C–O–C) functionalities. Further high binding energy components (*e.g.* C=O, 2.8–3.0 eV above the main peak, O–C=O, 3.6–4.3 eV above the main peak) can also be added if required. Spectra from insulating samples have been charge corrected to give the adventitious C 1s spectral component (C–C, C–H) a binding energy of 284.8 eV. This process has an associated error of ±0.1–0.2 eV [17]. Experience with numerous conducting samples and a routinely calibrated instrument has shown that the non-charge corrected C 1s signal generally ranges from 284.7 eV to as high as 285.2 eV [18]. The spectra for all (argon ion sputter cleaned) metallic species are referenced to Au $4f_{7/2}$ at 83.95 eV.

Spectra were analyzed using CasaXPS software [19] (version 2.3.14). Gaussian (*Y*%)–Lorentzian (*X*%), defined in CasaXPS as GL(*X*), profiles were used for each component. The best mixture of Gaussian–Lorentzian components is dependent on the instrument and resolution (pass energy) settings used as well as the natural line width of the specific core hole. For example, on the Kratos Axis Ultra at a 10 eV pass energy, the Mn $2p_{3/2}$ line for $KMnO_4$ is best fitted with a line shape of GL(75) while for spectra with broad peak shapes (*e.g.* Mn_2O_3) and/or satellite structure (*e.g.* MnO, $FeCO_3$, $Co(OH)_2$) line shapes of GL(30) are used for the individual components. The C 1s and O 1s peaks, which have large natural line widths, are also better fitted with a GL(30) line shape. Changes to the Gaussian–Lorentzian mix do not, in general, constitute large peak area changes for the fitting of mixed oxide systems (with the metal component being the exception). As long as the Gaussian–Lorentzian mix is in a reasonable range and applied consistently, reasonable results are obtained.

For metallic core lines, asymmetry was defined in the form of LA(α, β, m) where α and β define the spread of the tail on either side of the Lorentzian component. The parameter m specifies the width of the Gaussian used to convolute the Lorentzian curve. If values of α and β greater than unity are used the line shape will correct a problem with previous asymmetric line shapes [6,10,16] that tended to incorrectly estimate the peak area by incorporating area under the curve from binding energies well above the peak profile [20]. A standard Shirley background is used for all reference sample spectra.

Powder and metal samples of the highest purity readily available were purchased from Alfa Aesar. All powder samples were mounted on non-conductive adhesive tape. Metal samples were sputter cleaned using a 4 kV argon ion beam to remove all oxide and carbonaceous species. The powder samples were not sputter cleaned prior to analysis as it is well known that this can cause reduction of oxidized species. The NiO, NiOOH and $Ni(OH)_2$ sam-

ples are described in Ref. [5]. Cr_2O_3, $Cr(OH)_3$, eskolaite, chromite ($FeCr_2O_4$) and crocoite ($PbCrO_4$) samples are described in Ref. [10]. Iron oxide and oxy-hydroxides are described in Ref. [16]. All other powder samples were checked for purity by powder X-ray diffraction using an Inel diffractometer equipped with a XRG 3000 generator and CPS 120 curved position sensitive detector using monochromated Cu Kα radiation (λ = 1.54056 Å). A second set of both α-Fe_2O_3 (hematite) and γ-Fe_2O_3 (maghemite) (in addition to 16) were also analyzed using XRD and Raman spectroscopy (Renishaw 2000 Laser Raman spectrometer). Pure MnO was prepared by reducing both Mn_2O_3 and (separately) a commercially prepared MnO sample (that was shown to have slight surface oxidation) under a H_2 atmosphere at 1000 °C [21,22]. Manganite (MnO(OH), Morro da Mina, Brazil) and pyrolusite (MnO_2, Alberta, Michigan) samples were acquired from the Dana Mineral Collection at the University of Western Ontario (London, Ontario, Canada). All mineral samples were fractured in vacuum prior to analysis using a custom built cleaving device.

Powder and polycrystalline materials were used to remove the possibility of photoelectron diffraction effects which may result from single crystals, which can influence mulitplet splitting patterns [23,24]. These forms of sample are also more representative of the majority of samples examined during practical analyses of air-exposed multi-component materials.

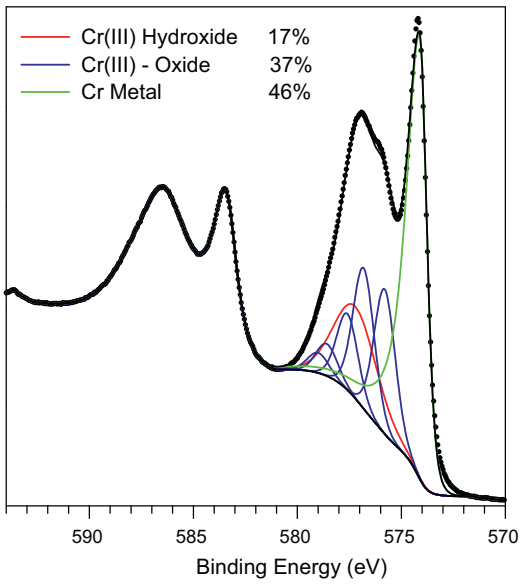

Fig. 1. An example of a Cr 2p spectrum fitted with parameters from Table 1. This spectrum is from a sample of a vacuum sputter deposited decorative chromium plated plastic and shows a thin layer of Cr_2O_3 and "$Cr(OH)_3$".

3. Results and discussion

3.1. Chromium

A primary objective of the interpretation of Cr 2p XP spectra is usually to determine the relative percentages present in the 0, II, III, IV and VI oxidation states in order to follow oxidation processes. These states have very different environmental toxicities in wastes, soils and processing products. In the past, misinterpretation of Cr 2p spectra has occurred due to the complex multiplet splitting that occurs for Cr(III) compounds. Stypula and Stoch [25] misinterpret the Cr(III) line shape and consequently identify both Cr^{3+} and "Cr^{n+} containing compounds". Desimoni et al. [26] present a survey of Cr containing reference materials, however all $2p_{3/2}$ peaks are fitted with a single peak of varying FWHM. The use of a single peak to represent the broad (non-symmetrical) peak shape of multiplet split Cr(III) species is used in numerous publications [27–31]. Halada and Clayton [32] and Grohmann et al. [33] attempt to use an asymmetric peak shape to model Cr(III) compounds. Halada and Clayton [32] have also analyzed a number of reference compounds including a prepared CrO_2 sample which they suggest gives rise to a single peak $2p_{3/2}$ binding energy at ≈575.2 eV. This appears to be contrary to accepted chemical shift theory which suggests Cr(IV) species have a binding energy higher than that for Cr(III) species (which Halada and Clayton list at a binding energy value of 576.3 eV). Halada and Clayton also fitted a number of peaks in the spectra to various different species. It is likely that some of these "species" would be better interpreted as multiplet structure. Brooks et al. [34] also use a series of single peaks to represent a series of chemical species including Cr(0), Cr_2O_3, CrOOH/$Cr(OH)_3$, CrO_3 and CrO_4^{2-} in a passive film on treated stainless steel (304 SS). However, RHEED data of the same sample does not detect Cr_2O_3, CrO_3 or CrO_4^{2-}. They further suggest that this is due to the species being disordered. Inspection of the spectra and comparison to later works [10,35] suggest that Cr(0) and $Cr(OH)_3$ are present with the broadened peak shape of the $Cr(OH)_3$ being incorrectly attributed to Cr(VI) species.

The poorer resolution of older XPS instruments may be one reason that a single peak shape has been taken to be of practical use. However, this may also play a part in misinterpretations of the species present. With newer generation instruments the fine multiplet structure is more often well resolved and must be taken into account. Some earlier publications [36,37] and now most later publications have recognized this [10,35] and employ multiple peaks to represent the various Cr(III) peak shapes.

For most publications, curve fitting of the different chemical states is rarely attempted. Our previous work [10] shows that systematic curve fitting of the various chemical states is possible provided suitable standard samples are examined and peak fitting parameters are fully reported. This work based the fitting of the multiplet peak structure on the theoretical modeling of Gupta and Sen [3] and the well-resolved standards spectra collected.

Fitting parameters for Cr $2p_{3/2}$ spectra (Table 1) are based on spectra taken from a series of well-characterized standard compounds. These fitting parameters have been slightly modified from those reported in our previous work [7,10]. The C 1s charge correction has been set to 284.8 eV (from 285.0 eV) and a new asymmetric peak shape for the metal has been defined. New analyses of Cr_2O_3 (powder), $FeCr_2O_4$ (chromite) and $NiCr_2O_4$ were carried out and are incorporated. Fitting parameters for Cr(0), Cr(III) oxide, Cr(III) hydroxide and Cr(VI) components were determined and these take into account asymmetry in the metal peak, a broader envelope of peaks attributed to multiplet splitting of the Cr(III) compounds and a single peak (no unpaired electrons) for Cr(VI) compounds. Cr(III) oxide shows discrete multiplet structure whereas the hydroxide shows only a broad peak shape. The asymmetry determined for the metal peak is based on spectra from an argon ion sputter cleaned pure metal surface. Peak FWHM for the Kratos Axis Ultra set at a pass energy of 20 eV are around 0.90 eV for the metal and the five individual Cr(III) oxide multiplet peaks, while the hydroxide peak FWHM is around 2.6 eV. Quantification of Cr(VI) species (single peak at 579.5 eV from average of literature data, FWHM of 1.3–1.5 eV to incorporate a variety of Cr(VI) species; or 579.6 eV for a standard CrO_3 sample, FWHM of 1.3–1.4 eV) is complicated by the overlap with the multiplet splitting of Cr(III) species. This is likely to result in an increase in the detection limit for Cr(VI), when present in a matrix dominated by Cr(III), to around 10% of the total Cr. Any contribution attributed to Cr(VI) below this value should be treated as below detection limits. An example of this type of fitting is presented in Fig. 1 which shows a Cr 2p spec-

Table 1
Cr $2p_{3/2}$ spectral fitting parameters: binding energy (eV), percentage of total area, FWHM value (eV) for each pass energy, and spectral component separation (eV).

Compound	Peak 1 (eV)	%	Peak 2 (eV)	ΔPeak 2 – Peak 1 (eV)[a]	%	Peak 3 (eV)	ΔPeak 3 – Peak 2 (eV)	%	Peak 4 (eV)	ΔPeak 4 – Peak 3 (eV)	%	Peak 5 (eV)	ΔPeak 5 – Peak 4 (eV)	%	FWHM, 10 eV pass energy	FWHM, 20 eV pass energy
Cr(0)[b]	574.2	100													0.80	0.90
Cr(III) Oxide[c]	575.7	36	576.7	1.01	35	577.5	0.78	19	578.5	1.00	8	578.9	0.41	5	0.88	0.94
Cr(III) hydroxide[d]	577.3	100													2.58	2.60
$FeCr_2O_4$ (Chromite)	575.9	41	577.0	1.09	39	577.9	0.88	13	578.9	1.04	7				1.12	1.20
$NiCr_2O_4$	575.2	35	576.2	1.02	34	577.0	0.81	18	578.1	1.05	9	579.2	1.13	4	1.09	
Cr(VI) mixed species[e]	579.5	100													1.40	1.50
Cr(VI) oxide[f]	579.6	100													1.28	1.38

[a] Binding energies are significant to 0.1 eV but an additional figure is added because energy splittings are much more accurate than the absolute binding energies.
[b] Asymmetric peak shape and FWHM defined by standard chromium metal sample (LA(1.3,4,5)).
[c] FWHM for multiplet splitting single peaks can be estimated by metal FWHM.
[d] This BE value is for an aged hydroxide, freshly prepared hydroxide has a BE of 577.1 eV.
[e] Binding energy from Literature average, broadened FWHM to incorporate a variety of Cr(VI) species.
[f] Binding energy and FWHM from standard CrO_3 sample.

Fig. 2. Cr 2p spectrum for a polished and sputter cleaned alloy I800 surface that has had a thin oxide film grown on it (10 Torr O_2, 6 min exposure, 300 °C). Peak fitting results in the assignment of mostly $FeCr_2O_4$ with some Cr_2O_3 and a small amount of the metallic phase.

trum from a vacuum sputter deposited Cr decorative coating. The percentage of the species present has been estimated from this fitting.

Fitting parameters from the new analyses of $FeCr_2O_4$ (chromite) and $NiCr_2O_4$ are presented in Table 1 and can be incorporated into a fitting scheme when these compounds may be present. The corresponding Fe 2p or Ni 2p spectra should also indicate the presence of these compounds in the appropriate (stoichiometric) amounts. An example of this is shown in Fig. 2 for a polished and sputter cleaned alloy I800 surface that has had a thin oxide film grown on it (10 Torr O_2, 6 min. exposure, 300 °C). The results for this (and similar samples) clearly show the formation of mostly $FeCr_2O_4$. Attempts to incorporate fittings for $Cr(OH)_3$ and Cr(IV) species do not result, after fitting iterations, in any significant amounts of these species. Inspection of the O 1s spectrum confirms the absence of the hydroxide. Survey spectra show that the surface is Fe rich with an Fe:Cr:Ni ratio of approximately 20:3:1, also lending support that the assignment for $FeCr_2O_4$ is correct. Fitting of Cr_2O_3 peaks in these spectra can result in varying resulting percentages that fluctuate depending on the background positioning and signal/noise of the spectrum. Due to the close overlap of peak positions and overall spectral shape for Cr_2O_3 and $FeCr_2O_4$ it is likely that meaningful separation by curve fitting of these two species requires extremely good spectral signal to noise. The use of a background with endpoints that are the average of the nearest five to eight data-points also greatly improves fitting repeatability.

3.2. Manganese

Manganese, having six stable oxidation states (0, II, III, IV, VI and VIII), three oxidation states with significant multiplet splitting (II, III, IV), one oxidation state with less defined splitting or broadening (VI), and overlapping binding energy ranges for these multiplet splitting structures, presents a serious challenge for both qualitative and quantitative analysis. Oku et al. [38] published a series of spectra of a variety of manganese oxide species. These spectra show excellent peak structure and are useful for qualitative assignment of Mn oxidation states. Some discussion of multiplet splitting is presented with some prominent peaks binding energy values reported, but no attempt at fitting of these structures is made. A thin layer

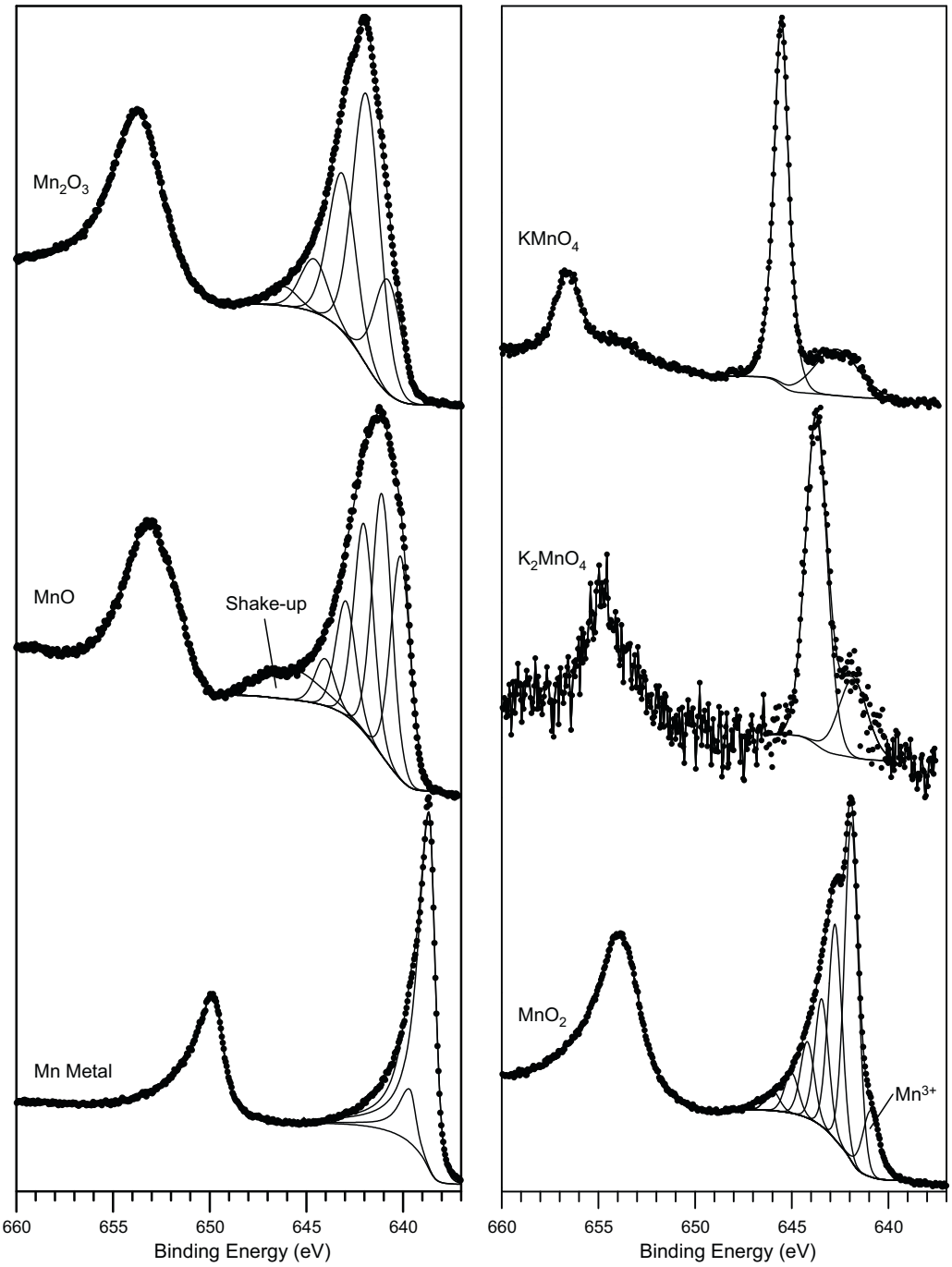

Fig. 3. Mn 2p spectra for (left, bottom) Mn metal, (left, middle) MnO, (left, top) Mn_2O_3, (right, bottom) MnO_2, (right, middle) K_2MnO_4, and (right, top) $KMnO_4$.

of nickel metal deposited on the surface of the samples is used for charge correction.

Nesbitt and Banerjee use curve fitting of Mn $2p_{3/2}$ spectra, based on the multiplet splitting proposed by Gupta and Sen [3], to interpret MnO_2 precipitation [11] and reactions on birnessite ($MnO_{1.7}(OH)_{0.25}$ or $MnO_{1.95}$) mineral surfaces [12–14]. These papers provide excellent detail of FWHM values, multiplet splitting separations and peak weightings for easy reproduction of their curve fitting procedure. Binding energies are quoted uncorrected for charging and the measured adventitious C 1s charge reference of 284.24 eV can only be found in one paper [12]. In the earlier publication [11], the authors include a small satellite peak at ≈645.5 eV in their fitting (≈10%, 3.5 eV FWHM) for MnO, but this is not discussed in later publications. Fitting parameters are based on standard spectra of MnO, natural manganite (MnOOH) and synthetic birnessite films (MnO_2) recorded on a Surface Science Laboratories SSX-100 X-ray photoelectron spectrometer equipped with a monochromatic Al Kα X-ray source. These fittings, with binding energies now corrected to adventitious C 1s at 284.8 eV (original data were shown uncorrected), are presented in Table 2. Also presented are peak parameters for a sputtered cleaned metal surface taken using the same instrument and analysis conditions.

Fitting parameters for recent spectra of the metal, and powder standards MnO, Mn_2O_3, MnO_2, K_2MnO_4 and $KMnO_4$, are presented in Table 3 with spectra for these standards given in Fig. 3. Spectra and fittings from in-vacuum fractured minerals specimens of manganite (MnOOH) and pyrolusite (MnO_2) are also presented (Fig. 4 and Table 3). These fittings are based on the parameters presented

Table 2
Mn $2p_{3/2}$ spectral fitting parameters compiled from references 11, 12, 13 and 14: binding energy (eV), percentage of total area, FWHM value (eV) for each pass energy, and spectral component separation (eV). Metal peak parameters were from spectra taken using the same Surface Science Laboratories SSX-100 X-ray photoelectron spectrometer and conditions as the above references.

Compound	Peak 1 (eV)	%	FWHM, SSX-100 25 eV pass energy	Peak 2 (eV)	Peak 2 – Peak 1 (eV)[a]	%	FWHM, SSX-100 25 eV pass energy	Peak 3 (eV)	Peak 3 – Peak 2 (eV)	%	FWHM, SSX-100 25 eV pass energy	Peak 4 (eV)	Peak 4 – Peak 3 (eV)	%	FWHM, SSX-100 25 eV pass energy	Peak 5 (eV)	Peak 5 – Peak 4 (eV)	%	FWHM, SSX-100 25 eV pass energy	Peak 6 (eV)	Peak 6 – Peak 5 (eV)	%	FWHM, SSX-100 25 eV pass energy
Mn(0)[b]	638.6	100.0	1.14																				
Mn(II), MnO[c]	640.3	34.4	1.70	641.5	1.20	26.2	1.70	642.3	0.80	16.9	1.70	643.2	2.50	8.6	1.70	647.5	4.29	3.5	1.70	645.0	−2.50	10.6	3.50
Mn(III), Manganite (MnOOH)	641.2	24.0	1.25	641.9	0.70	24.0	1.25	642.7	0.81	27.8	1.25	643.7	1.02	17.5	1.25	645.1	1.37	6.7	1.25				
Mn(IV), Birnessite (MnO_2)	642.5	47.9	1.25	643.5	1.02	30.6	1.3	644.3	1.3	45.3	1.3	645.3	1.03	4.8	1.3	646.4	1.02	2.9	1.25				

[a] Binding energies are significant to 0.1 eV but an additional figure is added because energy splittings are much more accurate than the absolute binding energies.
[b] Asymmetric peak shape and FWHM defined by standard manganese metal sample (LA(1.2,6.2,5)), result from this study.
[c] Peak 6 described as a satellite peak.

Table 3
Mn $2p_{3/2}$ spectral fitting parameters: binding energy (eV), percentage of total area, FWHM value (eV) for each pass energy, and spectral component separation (eV).

Compound	Peak 1 (eV)	%	Peak 2 (eV)	ΔPeak 2 – Peak 1 (eV)[a]	%	Peak 3 (eV)	ΔPeak 3 – Peak 2 (eV)	%	Peak 4 (eV)	Δ Peak 4 – Peak 3 (eV)	%	Peak 5 (eV)	ΔPeak 5 – Peak 4 (eV)	%	Peak 6 (eV)	ΔPeak 6 – Peak 5 (eV)	%	FWHM, 10 eV pass energy	FWHM, 20 eV pass energy
Mn(0)[b]	638.6	87.0	639.6	1.00	13.0													0.74	0.79
Mn(II) MnO[c]	640.2	24.0	641.1	0.97	27.8	642.1	0.93	22.1	643.0	0.95	12.5	644.2	1.14	4.7	645.9	1.75	9.1	1.21	1.23
Mn(III) Mn_2O_3	640.8	18.9	641.9	1.10	44.5	643.1	1.27	25.3	644.6	1.50	8.5	646.2	1.62	3.1				1.65	1.75
Mn(III) Manganite (MnOOH)	641.0	24.0	641.7	0.70	24.0	642.5	0.81	27.8	643.5	1.02	17.5	644.9	1.37	6.7				1.34	1.35
Mn(IV) MnO_2	641.9	41.7	642.7	0.86	26.5	643.4	0.70	15.5	644.2	0.75	9.1	645.0	0.85	4.9	646.0	1.00	2.5	0.84	0.91
Mn(IV) Pyrolusite (MnO_2)	641.8	21.0	642.7	0.87	27.4	643.5	0.75	16.1	644.3	0.81	8.9	645.2	0.91	4.6	646.2	1.03	2.1	0.92	0.99
Mn(VI) K_2MnO_4	643.8	100.0																1.31	1.40
Mn(VII) $KMnO_4$	645.5	100.0																0.98	1.08

[a] Binding energies are significant to 0.1 eV but an additional figure is added because energy splittings are much more accurate than the absolute binding energies.
[b] Both peaks have an asymmetric peak shape and FWHM defined by standard manganese metal sample (LA(1.1,3.2,3)).
[c] Peak 6 is a shake-up peak with FWHM of 3.5 eV (at both pass energies).

in Table 2 and modified as needed. In their later papers Banerjee and Nesbitt [12,13] also modify their fitting parameters, removing the satellite peak component from MnO and moving a peak (peak 5 for MnO in Table 2) to a binding energy of 4.4 eV above the first peak (peak 1). A narrower FWHM of 1.15 eV is used for each of the individual peaks for all three compounds (MnO, magnetite and birnessite).

The asymmetric Mn $2p_{3/2}$ main metal peak is found at 638.64 ± 0.06 eV with a $2p_{3/2}$ to $2p_{1/2}$ splitting of 11.10 ± 0.02 eV. This compares well to a NIST database average of 639.7 ± 1.0 eV and 11.15 ± 0.15 eV. Recent work [39] at the UE56/2-PGMI beamline at BESSY (synchrotron) has shown a well resolved second peak at ≈1 eV above the main peak which is attributed to an intra-atomic multiplet effect associated with Mn atoms with large local moment. This peak is also visible in the well resolved XPS spectrum shown in Fig. 3. It is fitted with a similar asymmetric peak shape as for the main peak, with an area of around 15% of the main peak. This peak is not discernable in the less well resolved spectra taken on the SSX-100 spectrometer.

Initial fitting of as-received MnO powder samples using Banerjee and Nesbitt's fitting parameters [12,13] indicated an extra component (≈641.1 eV) to be present. Inspection of the O 1s peak showed excess (≈42%) hydroxide which suggests the presence of $Mn(OH)_2$. Heating of this powder sample in vacuum to 400 °C for 16 h (similar to [38]) showed some decrease in the hydroxide/hydrate portion of the O 1s spectrum, however the well defined shake-up reported in the literature [11,40,41] is not resolved. There may also be some surface oxidation present. Pure MnO samples were then prepared by reducing separately both Mn_2O_3 and the as received MnO sample under a H_2 atmosphere at 1000 °C [21,22]. The resulting spectra from both these samples were similar to those reported previously in the literature.

Mn_2O_3 has a spectrum similar in binding energy range to MnOOH. The peak shape is slightly different for Mn_2O_3 which shows a small higher binding energy peak at 646.2 eV. Fitting parameters (Table 3) for MnOOH are similar to those from Nesbitt and Banerjee [11–14] in Table 2.

MnO_2 is fitted with 6 peaks of equal FWHM, compared to 5 peaks used by Nesbitt and Banerjee [11–14]. This is likely to be due to the much better resolution of the Kratos instrument used for the more recent analysis of this sample. The main resolved multiplet peak, as measured using the Kratos instrument, is too narrow (FWHM of 0.84 eV and 0.91 eV at 10 eV and 20 eV pass energies compared to 1.25 eV for SSX-100 spectrometer) when equal FWHM are used for the inclusion of 5 peaks to fit the entire spectrum and an extra peak is needed. As expected, vacuum fractured pyrolusite has a similar spectrum to the MnO_2 powder sample. Peak FWHM values are slightly greater (0.92 eV and 0.99 eV at 10 eV and 20 eV pass energies) and the relative concentration of Mn^{3+} is increased as well (≈10% Mn^{3+} in MnO_2 powder and ≈15% in pyrolusite). The small peak at the lower binding energy region of the spectra for both MnO_2 and pyrolusite can be shown to be a Mn^{3+} component and not part of the MnO_2 multiplet structure. Calculated spectra [3] do not show this peak and the relative peak intensity changes between the two samples. A timed analysis of MnO_2 powder shows that while MnO_2 is relatively stable in the incident X-ray beam (Al Kα 15 mA, 14 kV) the Mn^{3+} peak does grows from 6 to 14% of the total spectrum after 48 h of X-ray exposure. K_2MnO_4 gives rise to a slightly broadened peak (FWHM of 1.31 eV and 1.40 eV at 10 eV and 20 eV pass energies) at 634.8 eV compared to $KMnO_4$ (0.98 eV, 1.08 eV) at 645.5 eV.

3.3. Iron

For the analysis of photoelectron spectra of relatively pure iron oxides, one can use peak shape and peak binding energy

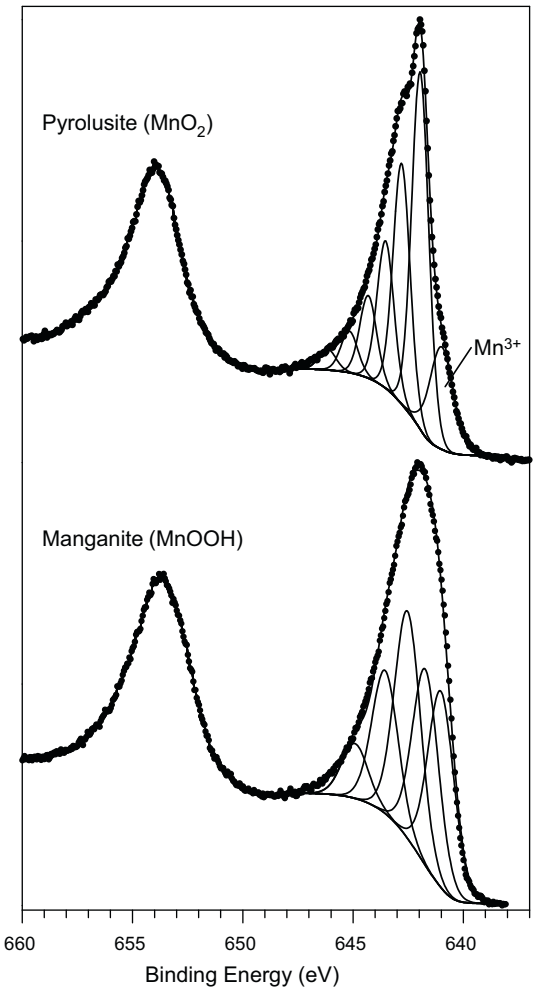

Fig. 4. Mn 2p spectra for (bottom) manganite (MnOOH) and (top) pyrolusite (MnO_2).

comparisons to standard compounds to derive oxide composition. McIntyre and Zetaruk's [15] paper is widely cited and is still an excellent starting point for qualitative iron oxide determination. A comparison of peak shapes to the theoretically calculated multiplet split peak shapes from Gupta and Sen [3] are discussed with relatively good agreement found. Pratt et al. [42] used a series of multiplet peaks to curve fit oxidized iron sulfide (pyrrhotite) surfaces. However, Lin et al. [43] used broad peak shapes to quantify Fe(0), Fe(II) and Fe(III) components in a series of thin oxide films. The authors used the shake-up satellites as approximate guides for the positioning of the main 2p peaks.

Grosvenor et al. [16] fitted the various iron oxide, hydroxide and halide peak shapes with a close approximation of the Gupta and Sen [3] multiplet structure. Multiplet FWHM, splittings and weightings are presented. An analysis of satellite to main peak separation is also given. All Fe(II) (high spin only as low spin Fe(II) does not exhibit multiplet splitting) and Fe(III) species can be fitted with Gupta and Sen multiplet structure. Variation in peak spacing and intensity occur for different ligands. Broad satellite peaks of varying intensities at binding energies above the main Fe $2p_{3/2}$ structure are present in the spectra for all high spin compounds. However paper [16] only presents the main multiplet lines, excluding the details needed to fit the broader higher binding energy satellite structures.

Table 4 presents full fitting parameters including the multiplet and satellite structure. FWHM values are reported for 10 eV pass energy only. To accommodate lower resolution settings slightly broader peaks would be necessary for best fit values. For these fits

Table 4
Fe $2p_{3/2}$ spectral fitting parameters: binding energy (eV), percentage of total area, FWHM value (eV) and spectral component separation (eV).

Compound	Peak 1 (eV)	FWHM, 10 eV pass energy	%	Peak 2 (eV)	ΔPeak 2 – Peak 1 (eV)[a]	FWHM, 10 eV pass energy	%	Peak 3 (eV)	ΔPeak 3 – Peak 2 (eV)	FWHM, 10 eV pass energy	%	Peak 4 (eV)	ΔPeak 4 – Peak 3 (eV)	FWHM, 10 eV pass energy	%	Peak 5 (eV)	ΔPeak 5 – Peak 4 (eV)	FWHM, 10 eV pass energy	%	Peak 6 (eV)	ΔPeak 6 – Peak 5 (eV)	FWHM, 10 eV pass energy	%
Fe(0)[b]	706.6	0.88	100.0																				
FeO	708.4	1.4	24.2	709.7	1.3	1.6	30.1	710.9	1.2	1.6	14.5	712.1	1.2	2.9	25.6	715.4	3.3	2.5	5.6				
α-Fe_2O_3	709.8	1.0	26.1	710.7	0.9	1.2	22.0	711.4	0.7	1.2	17.4	713.3	0.9	1.4	11.1	713.3	1.0	2.2	14.8	719.3	6.0	2.9	8.6
γ-Fe_2O_3	709.8	1.2	27.4	710.8	1.0	1.3	27.4	711.8	13.0	1.4	20.3	713.0	1.2	1.4	9.1	714.1	1.1	1.7	5.1	719.3	5.2	2.2	10.0
Ave. Fe_2O_3	**709.8**	**1.1**	**26.8**	**710.8**	**1.0**	**1.3**	**24.7**	**711.6**	**0.8**	**1.3**	**18.9**	**712.7**	**1.1**	**1.4**	**10.1**	**713.7**	**1.1**	**2.0**	**10.0**	**719.3**	**5.6**	**2.6**	**9.3**
Std. Dev.	0.0	0.1	0.9	0.1	0.1	0.1	3.8	0.3	0.2	0.1	2.1	0.5	0.2	0.0	1.4	0.6	0.1	0.4	6.9	0.0	0.6	0.5	1.0
α-FeOOH	710.2	1.3	26.7	711.2	1.0	1.2	25.3	712.1	0.9	1.4	21.0	711.2	1.21	1.4	12.1	714.4	1.2	1.7	7.2	719.8	5.4	3.0	7.7
γ-FeOOH	710.3	1.4	27.3	711.3	1.0	1.4	27.6	712.3	1.0	1.4	20.1	713.3	1.0	1.4	10.5	714.4	1.1	1.8	5.4	719.5	5.1	2.8	8.9
Ave. FeOOH	**710.3**	**1.4**	**27.0**	**711.3**	**1.0**	**1.3**	**26.5**	712.2	**0.9**	**1.4**	**20.6**	**713.3**	**1.1**	**1.4**	11.3	**714.4**	**1.1**	**1.8**	**6.3**	**719.7**	**5.3**	**2.9**	**8.3**
Std. Dev.	0.1	0.1	0.4	0.1	0.0	0.1	1.6	0.1	0.1	0.0	0.6	0.1	0.1	0.0	1.1	0.0	0.1	0.1	1.3	0.2	0.2	0.1	0.8
Average Fe(III)	**710.0**	**1.2**	**26.9**	**711.0**	**1.0**	**1.3**	**25.6**	**711.9**	**0.9**	**1.4**	**19.7**	**713.0**	**1.1**	**1.4**	**10.7**	**714.1**	**1.1**	**1.9**	**8.1**	**719.5**	**5.4**	**2.7**	**8.8**
Std. Dev.	0.3	0.2	0.6	0.3	0.30	0.1	2.6	0.4	0.1	0.1	1.6	0.5	0.1	0.0	1.3	0.5	0.1	0.2	4.5	0.2	0.4	0.4	0.9
$Fe_3O_4{}^{2+}$[c]	708.4	1.2	16.6	709.2	0.8	1.2	14.8																
$Fe_3O_4{}^{3+}$[c,d]	710.2	1.4	23.7	711.2	1.0	1.4	17.8	712.3	1.1	1.4	12.2	713.4	1.1	1.4	5.7	714.5	1.1	3.3	9.1	[c]			
$FeCr_2O_4$ (Chromite)[e]	709.0	2.0	40.5	710.3	1.2	1.5	12.9	711.2	0.9	1.5	17.8	713.0	1.2	1.5	8.3	713.8	1.4	3.6	20.6				
$NiFe_2O_4$	709.5	2.0	34.1	710.7	1.3	2.0	33.2	712.2	1.4	2.0	22.3	713.7	1.6	2.0	10.4								
$FeCO_3$ (Siderite)	709.8	1.5	24.3	711.1	1.3	1.5	13.2	712.0	0.9	3.6	41.9	715.6	3.6	3.4	20.0	719.4	3.8	1.5	0.70				

[a] Binding energies are significant to 0.1 eV but an additional figure is added because energy splittings are much more accurate than the absolute binding energies.
[b] Asymmetric peak shape and FWHM defined by standard iron metal sample (LA(1.2,4.8,3)).
[c] Sum of 2+ and 3+ areas is 100.
[d] Satellite structure for 3+ though likely present will be buried under Fe^{2+} Fe $2p_{1/2}$ portion of spectrum.
[e] Taken with a 20 eV pass energy.

Fig. 5. Fe 2p spectra for (bottom) chromite ($FeCr_2O_4$), (middle) $NiFe_2O_4$, and (top) siderite ($FeCO_3$).

a Shirley background encompassing only the $2p_{3/2}$ portion of the spectrum is used. Also included in this table are new spectral fitting parameters for $FeCr_2O_4$ and $NiFe_2O_4$, species that are important for the examination of oxide films on Fe–Cr–Ni alloys, as well as data for new analyses of α-Fe_2O_3 and γ-Fe_2O_3. Fitting parameters for $FeCO_3$, which has been noted in certain corrosion products, are also presented in Table 4 (Fe 2p spectra for $FeCr_2O_4$, $NiFe_2O_4$, and $FeCO_3$ are presented in Fig. 5). These analyses were collected from a mineral sample of siderite (cleaved in vacuum). Carbon 1s binding energy for $FeCO_3$ is at 290.1 eV.

While these values and reference spectra [15,16] will be useful for identification of pure oxide or oxy-hydroxide species, curve fitting of mixed systems quickly becomes complicated due to spectral overlaps. For example, it can be seen that various Fe(III) compounds have a similar range of Fe 2p binding energies and vary mostly in peak shape and satellite intensities. Any attempt at fitting two or more Fe(III) species to a spectrum will consequently contain an inherent degree of error. As well, overlap of the Fe(III) satellite structure with the Fe(0) and Fe(II) Fe $2p_{1/2}$ portion of the spectrum

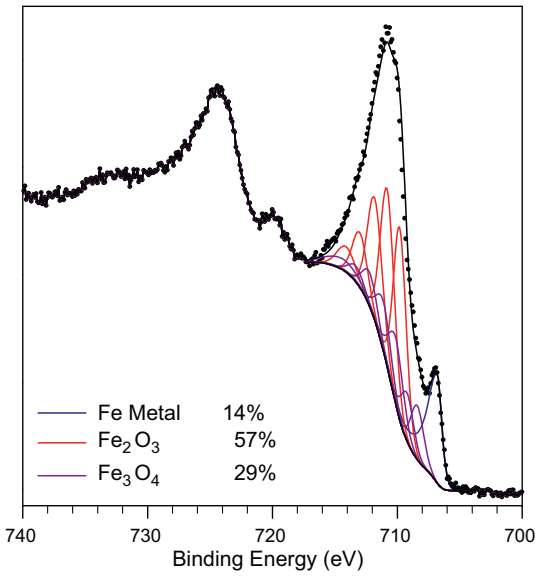

Fig. 6. Curve fitted Fe 2p spectrum of a mixed metal/oxide system of Fe based nanoparticles dispersed on a glass substrate.

will result in setting the higher binding energy background endpoint placement at a point that will not cover the satellite structure of the Fe(III) species. This will require any fitting of mixed chemical state systems containing Fe(III) species to omit the higher binding energy Fe(III) satellite from the envelope of peaks. This will again increase the error associated with the curve fitting. The fitting of a spectrum from pure Fe_3O_4 will also need to omit the higher binding Fe(III) energy satellite contribution as is reflected in the values presented in Table 4. Finally, determination of the Fe species present, especially in a mix of Fe(III) species, should include corroborating evidence from O 1s analysis and even other analytical techniques such as Raman spectroscopy or, for thin crystalline films, grazing angle XRD.

Fig. 6 presents an example of curve fitting of a mixed iron metal/oxide nano-particle system dispersed on a glass substrate. The resulting fit suggests a mix of metal, Fe_3O_4 and Fe_2O_3 components. The higher binding energy satellite peaks for Fe_2O_3 are omitted from the fitting, as are the assumed satellites for the Fe_3O_4 components. This will effectively cause a slight overestimation of the metal compared to the two oxide components. The O 1s spectrum confirms that the bulk of the O is present as a lattice oxide with only a small amount of hydroxide-like O detected.

Fig. 7 shows spectra of two polished carbon steel surfaces with electrochemically grown oxide (2.5 h, −0.2 V vs. SCE, pH 10.6, borate buffer solution) that has been treated with a 24 h bath of (A) 10^{-3} M and (B) 10^{-5} M H_2O_2. To determine the most representative Fe speciation the spectra were fitted with a variety of components. The peak fit residuals were examined after fitting with the metal component as well as the following species: (1) FeO, γ-Fe_2O_3 and FeOOH (average of two species), residuals of 4.28 and 3.79, for A and B, respectively, (2) Fe_3O_4 and γ-Fe_2O_3, residuals of 5.52 and 4.77, (3) Fe_3O_4 and Fe(III) average, residuals of 5.80 and 4.68, (4) FeO and γ-Fe_2O_3, residuals of 4.98 and 6.62, (5) Fe_3O_4, γ-Fe_2O_3 and FeOOH (average of two species), residuals of 4.61 and 4.02, (6) Fe_3O_4 and FeOOH (average of two species), residuals of 15.51 and 11.46, and (7) FeO, α-Fe_2O_3 and FeOOH (average of two species), residuals of 5.26 and 4.44. This iterative approach suggests that the best fit is found using a mix of FeO, γ-Fe_2O_3 and FeOOH components and is consistent with corrosion potential (E_{CORR}) results [44] on these surface layers where maghemite, rather than hematite, is implied. The error in the quantitation of this fit is likely to be large but com-

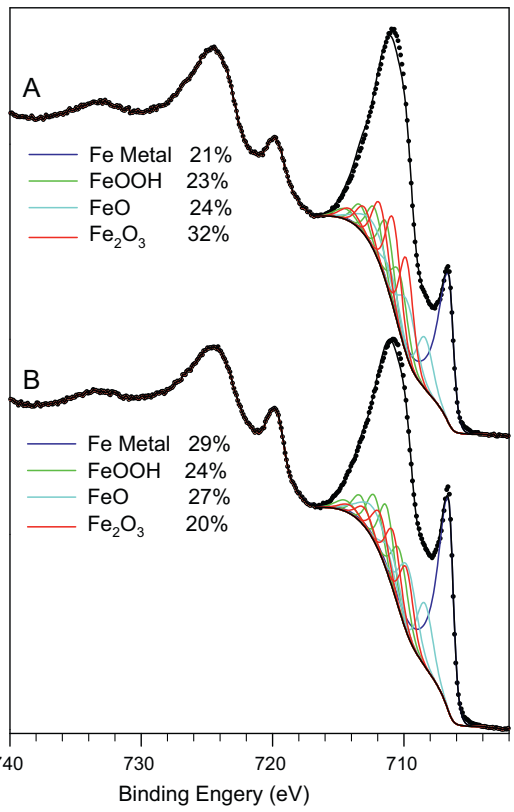

Fig. 7. Curve fitted Fe 2p spectra of two similar samples of a polished carbon steel surfaces with an electrochemically grown surface oxide (2.5 h, −0.2 V vs. SCE, pH 10.6, borate buffer solution) that has been treated with a 24 h bath of (A) 10^{-3} M and (B) 10^{-5} M H_2O_2.

plex fitting is still useful when comparisons of multiple samples with similar preparations are made (as is done here). An analysis of the O 1s spectra revealed that an increase in lattice oxide as compared to hydroxide is seen for sample A as compared to sample B, in agreement with the trend seen in the Fe $2p_{3/2}$ spectra.

Compared to the other transition metal species studied here, the complex multiple species fitting of Fe is the most problematic. With so many possible species having overlapping binding energies erroneous interpretation can result. A sample with two distinct species can likely be fitted accurately, three species much less so, while four or more species must be looked at as indicative but unreliable. It is worth again stating that corroborating evidence is desirable for this type of Fe surface chemical state speciation.

3.4. Cobalt

There appears to be few instances of good quality high-resolution Co 2p spectra presented in the literature. Fitting appears to be inconsistent with generally only a qualitative approach to the analysis of the spectral changes reported. Fitting of a broad main peak combined with a portion of the satellite structure has been one approach [45,46] although fitting parameter details are not presented in enough detail to emulate.

Recent work [47] has clarified the position and type of plasmon loss structure associated with the Co metal (and CoP, cobalt phosphide) spectrum. The Co metal spectrum is fitted with an asymmetric main peak and two plasmon loss peaks at 3.0 eV and 5.0 eV above the main peak, which constitute the surface and bulk plasmons, respectively, with FWHM values of 3.0 eV in both cases.

Obtaining a pure CoO specimen was problematic. Initial analysis of a commercial CoO sample showed the surface to be extensively

Table 5
Co $2p_{3/2}$ spectral fitting parameters: binding energy (eV), percentage of total area, FWHM value (eV) for each pass energy, and spectral component separation (eV).

Compound	Peak 1 (eV)	%	Peak 1 FWHM, 10 eV pass energy	Peak 1 FWHM, 20 eV pass energy	Peak 2 (eV)	Δ Peak 2 – Peak 1 (eV)[a]	%	Peak 2 FWHM, 10 eV pass energy	Peak 2 FWHM, 20 eV pass energy	Peak 3 (eV)	Δ Peak 3 – Peak 2 (eV)	%	Peak 3 FWHM, 10 eV pass energy	Peak 3 FWHM, 20 eV pass energy	Peak 4 (eV)	Δ Peak 4 – Peak 3 (eV)	%	Peak 4 FWHM, 10 eV pass energy	Peak 4 FWHM, 20 eV pass energy	Peak 5 (eV)	Δ Peak 5 – Peak 4 (eV)	%	Peak 5 FWHM, 10 eV pass energy	Peak 5 FWHM, 20 eV pass energy
Co(0)[b]	778.1	81.0	0.70	0.75	781.1	3.00	11.0	3.00	3.00	783.1	2.00	8.0	3.00	3.00											
CoO	780.0	46.6	2.23	2.24	782.1	2.10	25.7	2.59	2.66	785.5	3.40	1.6	2.42	2.29	786.5	1.00	26.1	5.28	4.98						
$Co(OH)_2$	780.4	38.1	2.01	2.04	782.2	1.80	26.6	2.60	2.55	786.0	3.79	33.0	4.47	4.47	790.4	4.40	2.4	2.33	2.33						
CoOOH[c]	780.1	61.4		1.48	781.4	1.32	24.5		1.48	783.1	1.68	5.2		1.48	790.1	7.07	8.9		3.30						
Co_3O_4	779.6	40.5	1.38	1.39	780.9	1.30	29.1	1.55	1.62	782.2	1.30	15.2	1.94	2.18	785.2	3.00	8.1	4.28	4.44	789.5	4.30	7.2	3.15	3.29

[a] Binding energies are significant to 0.1 eV but an additional figure is added because energy splittings are much more accurate than the absolute binding energies.
[b] Asymmetric peak shape (Peak 1) and FWHM defined by standard cobalt metal sample LA(1.2,5,5), LMM B Auger peak seen at 766.2 eV, 2.2 eV FWHM.
[c] From a fit of a digitized copy from reference 54.

Fig. 8. Co 2p spectra for (bottom to top) Co metal, CoO, $Co(OH)_2$ and Co_3O_4.

oxidized to Co_3O_4 even though the bulk powder XRD spectrum showed only CoO. This appears to be a common problem with two published databases [2,48] showing similar Co_3O_4 oxidized surfaces for CoO. Attempts to reduce this surface oxide by heating the sample to 950 °C (4 h) under argon were unsuccessful. A second sample purchased from the same supplier contained larger lumps of the compound that when ground by mortar and pestle and analyzed gave spectra that were more consistent with literature results. To confirm this, spectra from three different literature sources [49–51] were digitized, curve fitted and compared to our results. The areas of the main peak centered at ≈780 eV relative to the satellite peak at ≈786 eV were compared and were shown to

Table 6
Ni $2p_{3/2}$ spectral fitting parameters: binding energy (eV), percentage of total area, FWHM value (eV) for each pass energy, and spectral component separation (eV).

Compound	Peak 1 (eV) a)	%	Peak 1, FWHM, 10 eV pass energy	Peak 1, FWHM, 20 eV pass energy	Peak 2 (eV)	ΔPeak 2 – Peak 1 (eV)[a]	%	Peak 2, FWHM, 10 eV pass energy	Peak 2, FWHM, 20 eV pass energy	Peak 3 (eV)	ΔPeak 3 – Peak 2 (eV)	%	Peak 3, FWHM, 10 eV pass energy	Peak 3, FWHM, 20 eV pass energy	Peak 4 (eV)	ΔPeak 4 – Peak 3 (eV)	%	Peak 4, FWHM, 10 eV pass energy	Peak 4, FWHM, 20 eV pass energy
Ni Metal from [5][b,d]	852.6	79.6	1.00	1.02	856.3	3.65	5.6	2.48	2.48	858.7	2.38	14.8	2.48	2.48					
Ni Metal - New Line Shape[c,d]	852.6	81.2	0.94	0.95	856.3	3.65	6.3	2.70	2.70	858.7	2.38	12.5	2.70	2.70					
NiO	853.7	14.3	0.98	1.02	855.4	1.71	44.2	2.04	3.25	860.9	5.44	34.0	3.85	3.76	864.0	3.10	3.6	1.97	2.04
$Ni(OH)_2$	854.9	7.4	1.12	1.16	855.7	0.77	45.3	1.5	2.29	857.7	2.02	3.0	1.59	1.59	860.5	2.79	1.4	1.06	1.06
Gamma NiOOH	854.6	13.8	1.40		855.3	0.70	12.4	6.50		855.7	0.36	9.7	1.40		856.5	0.78	20.7	1.40	
Beta NiOOH (3+ Portion)[e]	854.6	9.2	1.40		855.3	0.70	8.3	5.30		855.7	0.36	6.4	1.40		856.5	0.78	13.8	1.40	
Beta NiOOH (2+ Portion)[e]	854.9	2.5	1.12		855.7	0.77	15.1	1.5		857.7	2.02	1.0	1.59		860.5	2.79	0.5	1.06	
$NiCr_2O_4$	853.8	7.0	1.22	1.30	855.8	1.95	20.5	1.82	1.86	856.5	0.71	24.7	3.91	7.01	861.0	4.50	2.3	1.27	1.33
$NiFe_2O_4$	854.5	17.3	1.35	1.36	856.0	1.52	38.2	3.03	2.98	861.4	5.41	38.5	4.49	4.50	864.7	3.29	2.8	3.04	3.01

Compound	Peak 5 (eV)	ΔPeak 5 – Peak 4 (eV)	%	Peak 5, FWHM, 10 eV pass energy	Peak 5, FWHM, 20 eV pass energy	Peak 6 (eV)	ΔPeak 6 – Peak 5 (eV)	%	Peak 6, FWHM, 10 eV pass energy	Peak 6, FWHM, 20 eV pass energy	Peak 7 (eV)	ΔPeak 7 – Peak 6 (eV)	%	Peak 7, FWHM, 10 eV pass energy	Peak 7, FWHM, 20 eV pass energy
Ni Metal from [5][b,d]															
Ni Metal - New Line Shape[c,d]															
NiO	866.3	2.38	3.9	2.60	2.44										
$Ni(OH)_2$	861.5	1.00	39.2	4.64	4.65	866.5	4.96	3.7	3.08	3.01					
Gamma NiOOH	857.8	1.33	8.7	1.90		861.0	3.20	23.3	4.00		864.4	3.38	11.4	4.40	
Beta NiOOH (3+ Portion)[e]	857.8	1.33	5.8	1.90		861.0	3.20	15.6	4.00		864.4	3.38	7.6	4.40	
Beta NiOOH (2+ Portion)[e]	861.5	1.00	13.1	4.64		866.5	4.96	1.2	3.08						
$NiCr_2O_4$	861.3	0.26	39.4	4.34	4.31	866.0	4.73	6.1	2.07	2.13					
$NiFe_2O_4$	867.0	2.27	3.2	2.61	2.66										

[a] Binding energies are significant to 0.1 eV but an additional figure is added because energy splittings are much more accurate than the absolute binding energies.
[b] Asymmetric peak shape for peak 1 defined by standard nickel metal sample, CasaXPS peak shape parameter = A(0.4,0.55,10)GL(30).
[c] Asymmetric peak shape for peak 1 defined by standard nickel metal sample, CasaXPS peak shape parameter = LA(1.1,2.2,10).
[d] Metal peak is corrected to $Au4f_{7/2}$ set to 83.95 eV. All other peaks are charge corrected to C 1s (C–C, C–H, adventitious carbon) set to 284.8 eV.
[e] Beta NiOOH has a ratio of 2:1 Ni(III):Ni(II). Peak percentages for the 3+ and 2 + portions for Beta NiOOH total 100%.

Table 7
Selected O 1s values.

Compound	O 1s lattice oxide	Std. Dev. (±eV)	%	FWHM, 10 eV pass energy	FWHM, 20 eV pass energy	O 1s hydroxide, hydrated or defective oxide	Std. Dev. (±eV)	%	FWHM, 10 eV pass energy	FWHM, 20 eV pass energy	O 1s water, organic O	Std. Dev. (±eV)	%	FWHM, 10 eV pass energy	FWHM, 20 eV pass energy
Cr(III) Cr_2O_3 - Vacuum Fractured	530.12	0.00	42	0.84	0.89	530.90	0.01	58	3.15	3.08					
Cr(III) Cr_2O_3 - Air Exposed	530.10	0.11	56	1.19	1.34	531.83	0.04	41	2.50	2.12	533.82	0.21	3	2.50	2.12
Cr(III) Eskolaite, Cr_2O_3	529.86	0.04	33	1.13	1.16	531.15	0.06	64	1.80	1.79	533.19	0.05	4	1.80	1.79
Cr(III) "$Cr(OH)_3$"						531.70	0.10	88	1.68		533.43	0.10	12	1.42	
Cr(VI) CrO_3	530.37	0.08	66	1.17	1.18	531.47	0.16	26	1.53	1.86	533.01	0.04	8	1.53	1.86
Cr(VI) Crocoite, CrO_3	529.90		82		1.01	530.88		18		1.99					
Mn(II) MnO	529.96	0.05	66	1.00	1.001	531.25	0.10	34	1.91	2.06					
Mn(III) Mn_2O_3	529.97	0.08	72	1.03	1.07	531.63	0.04	24	1.62	1.62	533.07	0.15	3	1.62	1.62
Mn(III) Manganite, MnO(OH)	529.96	0.04	46	1.17	1.21	531.19	0.04	44	1.17	1.21	532.29	0.08	10	1.17	1.21
Mn(IV) MnO_2	529.54	0.05	63	0.81	0.88	530.41	0.16	16	1.97	2.13	532.08	0.07	21	1.97	2.13
Mn(IV) Pyrolusite, MnO_2	529.51	0.08	54	0.88	0.92	531.61	0.13	25	2.14	2.11	531.86	0.27	21	2.14	2.11
Mn(VI) K_2MnO_4	530.56	0.05	100	1.32	1.40										
Mn(VII) $KMnO_4$	530.69	0.07	100	1.00	1.10										
Fe(II) FeO	529.96	0.25	59	0.97		531.36	0.08	28	1.25		532.23	0.04	13	1.25	
Fe(III) α-Fe_2O_3	529.88	0.06	60	1.12		531.26	0.14	31	1.57		532.49	0.30	10	1.57	
Fe(III) γ-Fe_2O_3	529.94	0.10	61	1.15		531.74	0.10	28	1.58		533.29	0.10	11	1.58	
Fe(III) α-FeOOH	529.90		39	1.11		531.20		49	1.11		532.50		12	1.11	
Fe(III) γ-FeOOH	529.90		40	1.21		531.30		37	1.21		532.30		15	1.21	
Fe(II,III) Fe_3O_4	530.11	0.10	42	0.88		530.94	0.10	43	1.87		532.67	0.10	16	1.87	
Fe(II) Cr(III) $FeCr_2O_4$	530.22	0.28	46	0.95	0.98	531.31	0.02	54	2.30	2.30					
NI(II) Fe(III) $NiFe_2O_4$	529.80	0.07	54	1.38	1.48	531.76	0.04	46	2.25	2.20					
Co(II) CoO	529.79	0.10	62	1.00	1.01	531.37	0.12	34	1.58	1.65	532.87	0.14	4	1.58	1.65
Co(II) $Co(OH)_2$						531.07	0.03	86	1.37	1.39	532.25	0.06	14	1.37	1.39
Co(II,III) Co_3O_4	529.95	0.12	53	0.72	0.78	530.84	0.02	41	2.13	2.28	532.66	0.05	6	2.13	2.28
Ni(II) NiO	529.30	0.04	69	0.85	0.92	531.10	0.04	29	1.50	1.50	532.80	0.10	2	1.50	1.50
Ni(II) $Ni(OH)_2$						530.90	0.10	100	1.46	1.46					
NI(II) Cr(III) $NiCr_2O_4$	529.99	0.01	64	0.94		530.95	0.05	36	2.16						

[a] For this species there is a higher binding energy peak at 533.5 eV (1.21 eV FWHM), 8% ascribed to physisorbed water.

be equivalent. The results presented here show significantly better resolution than previous work using non-monochromatic sources [49,50,52,53] and/or older spectrometers [51].

Co metal, CoO, $Co(OH)_2$ and Co_3O_4 spectra are presented in Fig. 8 with spectral fitting parameters given in Table 5. Fitting parameters for CoOOH from a fit of a digitized spectrum from the recent work of Yang et al. [54] are also presented. As for Fe, the binding energy overlap of the various oxide and hydroxide forms will greatly increase the absolute error in speciation quantitation. However, curve fitting procedures such as those presented here, should be useful for a more meaningful interpretation for a series of similar Co containing samples. A second concern is the overlap of the higher binding energy $2p_{3/2}$ multiplet or satellite structures of the various oxides and hydroxides with the metal $2p_{1/2}$ peak at 793.1 eV. This overlap, when the metal is present, requires the use of an offset for the higher binding energy background endpoint similar to that used for Ni as described previously [5] and in the section below.

3.5. Nickel

There is a large body of work based on the use of XPS for the examination of Ni metal, oxide and alloy surfaces with varying methods of chemical state identification used with moderate to good success. For much of the earlier work the importance of multiplet splitting and satellite structure in the interpretation of the Ni 2p line shape was understood but limited models for fitting these structures were available [55,56]. Recent experimental and theoretical advances have considerably improved the fitting process. Our recent publications [5,6] summarizes some of the important milestones in these works which will not be duplicated here. The curve fitting method [5] will be summarized here and the work expanded to include the important nickel ferrite and nickel chromite species which are particularly important for the understanding of corrosion chemistry of Ni alloys. This recent work [5,57] and others works [58,59] shows how spectral subtraction using quality reference spectra can be used to identify small amounts of Ni(III) within the complex spectral profile of NiO in thin oxide films.

These curve fitting techniques [5] use specified empirical fitting parameters that take into account the unique peak shapes of the various Ni compounds. Spectra are fitted with the asymmetric line shape and plasmon loss peaks for Ni metal and an empirical fit of the NiO and $Ni(OH)_2$ line shapes from parameters derived from standard samples (Table 6). The binding energy differences, FWHM and area ratios are constrained for each species. The absolute binding energy values were allowed to vary by ±0.1 eV to allow for error associated with charge referencing to adventitious C 1s. Overlap of the high binding energy satellite structure from $Ni(OH)_2$ (and to a lesser extent NiO) with the $2p_{1/2}$ metal peak, which is composed of an asymmetric main peak and contributions from plasmon loss structure, can make the definition of an appropriate spectral background using only the $2p_{3/2}$ portion of the spectrum problematic. This work [5] has shown that a Shirley background applied across the entire 2p ($2p_{3/2}$ and $2p_{1/2}$) portion of the spectrum works reasonably well (even though fitting of only the $2p_{3/2}$ portion of spectrum is carried out). In many cases an offset of the higher binding energy end of the background can be used to improve the fit of the peak shapes. The appropriate background offset is determined using an iterative approach while monitoring a residual plot of the $2p_{3/2}$ area. It is necessary during spectral acquisition to use a window of sufficient width (848.0–890.0 eV) to accurately assess the end of the Ni $2p_{1/2}$ envelope for positioning of the background endpoint.

The present work extends this approach to include fitting parameters for $NiCr_2O_4$ and $NiFe_2O_4$, with fitting parameters presented in Table 6. Ni 2p spectra of these two species are provided in Fig. 9.

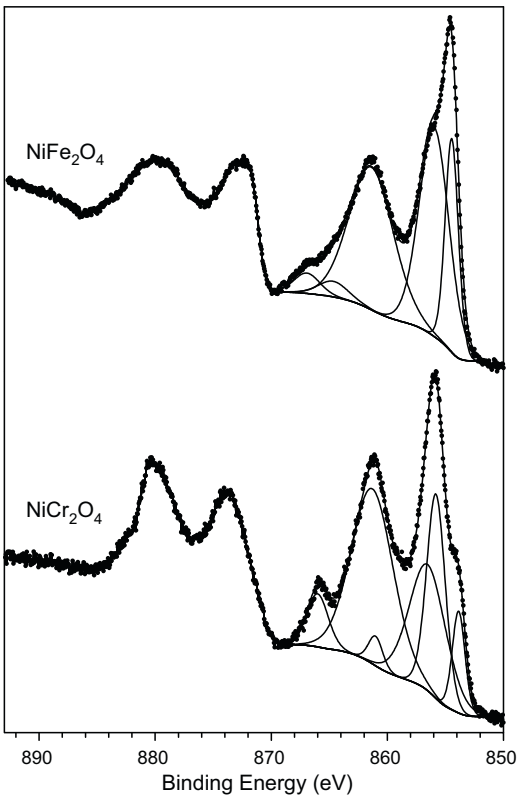

Fig. 9. Ni 2p spectra for (bottom) $NiCr_2O_4$ and (top) $NiFe_2O_4$.

3.6. Oxygen

The O 1s binding energy and FWHM values obtained for the standard samples are presented in Table 7. For many of the pure oxide samples there is a second higher binding energy peak that can be attributed to contributions from a defective oxide component inherent in these oxide surfaces as suggested previously [5] and not an hydroxide as this has been ruled out by other methods [60,61]. For all of the oxides studied here this peak has an area contribution between 20 and 40% consistent with other powdered oxides including those of Ni [5] and Cr [10]. There was also no difference in this peak area between a Cr_2O_3 lump fractured in vacuum [10] and powdered samples mounted on conductive tape (this work). These contributions from defective sites are unlikely to compromise the assignment of chemical states. It should be noted that this second peak could also result from carbonate species arising from reaction with CO_2 during air exposure [1,2]. Inspection of the C 1s spectrum should confirm if this is the case.

Pure oxide samples were not heated to remove possible surface hydroxides before analysis to avoid reduction of the oxide. In one related experiment in this laboratory with MnO heated to 600 °C for 12 h, there was no significant change in the higher binding energy component attributed to defective oxide, indicating little or no surface hydroxide was present.

4. Conclusions

Analysis of the X-ray photoelectron 2p spectra of the first row transition metals is challenging due to peak asymmetries, complex multiplet splitting, shake-up and plasmon loss structure, and uncertain, overlapping binding energy positions. Practical curve fit-

ting and quantification procedures for the various chemical states of Cr, Mn, Fe, Co and Ni containing samples have been presented. These procedures are based on a critical evaluation of existing literature and on high-resolution analyses of well-characterized standards. A full report of binding energies, full-width at half maximum values, spin–orbit splitting values, and asymmetric peak shape fitting parameters (for conductive species) has been presented and, when constrained appropriately, will allow consistent curve fitting of spectra from a variety Cr, Mn, Fe, Co and Ni containing compounds or surfaces. These procedures are relatively simple to implement and have been found to be reliably reproducible across a wide range of samples. We also provide examples where these more detailed fitting procedures can be used to resolve and quantify various chemical states in transition metals and compounds where previous fitting without recognition of multiplet contributions has been inadequate.

Acknowledgments

The Kratos Axis Ultra was funded in part by a Canadian Foundation for Innovation (CFI) grant. The nano-Fe sample was courtesy of Ms. Ruchi Shah, Dept. of Civil and Environmental Engineering at U.W.O. The electrochemically grown and H_2O_2 treated iron oxide samples were courtesy of Mr. Kevin Daub, Dept. of Chemistry at U.W.O. Siderite (iron carbonate) sample was supplied by Dr. Allen Pratt, CanMET Laboratories (Ottawa). Thanks to Mr. Brad Kobe, Dr. Michael Jennings and Dr. Allen Pratt for their assistance with the XRD analyses and Ms. Mary Jane Walzak with the Raman analyses of the standard samples.

References

[1] C.D. Wagner, A.V. Naumkin, A. Kraut-Vass, J.W. Allison, C.J. Powell, J.R.Jr. Rumble, NIST Standard Reference Database 20, Version 3.4 (web version) (http://srdata.nist.gov/xps/) 2003.
[2] J.F. Moulder, W.F. Stickle, P.E. Sobol, K.D. Bomben, Handbook of X-ray Photoelectron Spectroscopy, Perkin-Elmer Corp., Eden Prairie, MN, 1992.
[3] R.P. Gupta, S.K. Sen, Phys Rev. B 12 (1975) 12.
[4] M.C. Biesinger, L.W.M. Lau, A.R. Gerson, R.St.C. Smart, Appl. Surf. Sci. 257 (2010) 887.
[5] M.C. Biesinger, B.P. Payne, L.W.M. Lau, A.R. Gerson, R.St.C. Smart, Surf. Interface Anal. 41 (2009) 324.
[6] A.P. Grosvenor, M.C. Biesinger, R.St.C. Smart, N.S. McIntrye, Surf. Sci. 600 (2006) 1771.
[7] M.C. Biesinger, B.P. Payne, B.R. Hart, A.P. Grosvenor, N.S. McIntyre, L.W.M. Lau, R.St.C. Smart, J. Phys. Conf. Ser. 100 (2008) 012025.
[8] H. Ye, X.Y. Liu, H. Hong, Mater. Sci. Eng. C 29 (2009) 2036.
[9] H. Ye, X.Y. Liu, H. Hong, Appl. Surf. Sci. 255 (2009) 8134.
[10] M.C. Biesinger, C. Brown, J.R. Mycroft, R.D. Davidson, N.S. McIntyre, Surf. Interface Anal. 36 (2004) 1550.
[11] H.W. Nesbitt, D. Banerjee, Am. Miner. 83 (1998) 305.
[12] D. Banerjee, H.W. Nesbitt, Geochim. Cosmochim. Acta 63 (1999) 3025.
[13] D. Banerjee, H.W. Nesbitt, Geochim. Cosmochim. Acta 63 (1999) 1671.
[14] D. Banerjee, H.W. Nesbitt, Geochim. Cosmochim. Acta 65 (2001) 1703.
[15] N.S. McIntyre, D.G. Zetaruk, Anal. Chem. 49 (1977) 1521.
[16] A.P. Grosvenor, B.A. Kobe, M.C. Biesinger, N.S. McIntyre, Surf. Interface Anal. 36 (2004) 1564.
[17] D.J. Miller, M.C. Biesinger, N.S. McIntyre, Surf. Interface Anal. 33 (2002) 299.
[18] M.C. Biesinger, Unpublished Results, University of Western Ontario, London, ON, Canada, 1995–2010.
[19] N. Fairley, http://www.casaxps.com, ©Casa software Ltd., 2005.
[20] N. Fairley CasaXPS, Personal Communication, 2007.
[21] R.W. Millar, J. Amer. Chem. Soc. 50 (1928) 1875.
[22] J.C. Southard, C.H. Shomate, J. Amer. Chem. Soc. 64 (1942) 1770.
[23] D. Briggs, J.C. Rivière, Spectral interpretation, in: D. Briggs, M.P. Seah (Eds.), Practical Surface Analysis by Auger and X-ray Photoelectron Spectroscopy, John Wiley & Sons, Chichester, UK, 1983, p. 135.
[24] P.A.W. Van der Heide, J. Electron Spectrosc. Relat. Phenom. 164 (2008) 8.
[25] B. Stypula, J. Stoch, Corros. Sci. 36 (1994) 2159.
[26] E. Desimoni, C. Malitesta, P.G. Zambonin, J.C. Rivière, Surf. Interface Anal. 13 (1988) 173.
[27] V. Maurice, W.P. Yang, P. Marcus, J. Electrochem. Soc. 141 (1994) 3016.
[28] D.R. Rosseinsky, G.K. Muthakia, C.L. Honeybourne, R.L. Ewen, Transit. Met. Chem. 20 (1995) 88.
[29] E. Kemnitz, A. Kohne, I. Grohmann, A. Lippitz, W.E.S. Unger, J. Catal. 159 (1996) 270.
[30] X.Y. Li, E. Akiyama, H. Habazaki, A. Kawashima, K. Asami, K. Hashimoto, Corros. Sci. 39 (1997) 1365.
[31] M. Tetsuya, K. Takao, J. Shimomura, Appl. Surf. Sci. 121/122 (1997) 120.
[32] G.P. Halada, C.R. Clayton, J. Electrochem. Soc. 138 (1991) 2921.
[33] I. Grohmann, E. Kemnitz, A. Lippitz, Surf. Interface Anal. 23 (1995) 887.
[34] A.R. Brooks, C.R. Clayton, K. Doss, Y.C. Lu, J. Electrochem. Soc. 133 (1986) 2459.
[35] E. Ünveren, E. Kemnitz, S. Hutton, A. Lippitz, W.E.S. Unger, Surf. Interface Anal. 36 (2004) 92.
[36] N.S. McIntyre, T.C. Chan, C. Chen, Oxid. Met. 33 (1990) 457.
[37] A.R. Pratt, N.S. McIntyre, Surf. Interface Anal. 24 (1996) 529.
[38] M. Oku, K. Hirokawa, S. Ikeda, J. Electron Spectrosc. Rel. Phenom. 7 (1975) 465.
[39] A.K. Shukla, P. Krüger, R.S. Dhaka, D.I. Sayago, K. Horn, S.R. Barman, Phys. Rev. B 75 (2007) 235419.
[40] V. Di Castro, G. Polzonetti, J. Electron Spectrosc. Rel. Phenom. 48 (1989) 117.
[41] K. Okada, A. Kotani, J. Phys. Soc. Jpn. 61 (1992) 4619.
[42] A.R. Pratt, I.J. Muir, H.W. Nesbitt, Geochim. Cosmochim. Acta 58 (1994) 827.
[43] T.C. Lin, G. Seshadri, J.A. Kelber, Appl. Surf. Sci. 119 (1997) 83.
[44] K. Daub, X. Zhang, D. Shoesmith, J.C. Wren, Meet Abtr. – Electrochem. Soc. 901 (2009) 643.
[45] J.C. Dupin, Thin Solid Films 384 (2001) 23.
[46] A. Foelske, H.H. Strehblow, Surf. Interface Anal. 29 (2000) 548.
[47] A.P. Grosvenor, S.D. Wik, R.G. Cavell, A. Mar, Inorg. Chem. 44 (2005) 8988.
[48] B.V. Crist, Handbook of Monochromatic XPS Spectra, Vol. 2 Commercially Pure Binary Oxides, XPS International Inc., 1999, pp. 72–78.
[49] N.S. McIntrye, M.G. Cook, Anal. Chem. 47 (1975) 2208.
[50] J. van Elp, J.L. Wieland, H. Eskes, P. Kuiper, G.A. Sawatzky, F.M.F. De Groot, T.S. Turner, Phys. Rev. B 44 (1991) 6090.
[51] H. Yang, J. Ouyang, A. Tang, J. Phys. Chem. B 111 (2007) 8006.
[52] M.A. Langell, F. Gevrey, M.W. Nydegger, Appl. Surf. Sci. 153 (2000) 114.
[53] V.M. Jiminez, J.P. Espinos, A.R. González-Elipe, Surf. Interface Anal. 26 (1998) 62.
[54] J. Yang, H. Liu, W.N. Martens, R.L. Frost, J. Phys. Chem. C 114 (2010) 111.
[55] M.W. Roberts, R.St.C. Smart, J. Chem. Soc., Faraday Trans. 80 (1984) 2957.
[56] N.S. McIntyre, D.G. Zetaruk, D. Owen, Appl. Surf. Sci. 2 (1978) 55.
[57] B.P. Payne, M.C. Biesinger, N.S. McIntyre, J. Electron Spectrosc. Rel. Phenom. 175 (2009) 55.
[58] A.F. Carley, S.D. Jackson, J.N. O'Shea, M.W. Roberts, Surf. Sci. 440 (1999) L868.
[59] B.P. Payne, A.P. Grosvenor, M.C. Biesinger, B.A. Kobe, N.S. McIntyre, Surf. Interfece Anal. 9 (2007) 582.
[60] H.A.E. Hagelin-Weaver, J.F. Weaver, G.B. Hoflund, G.N. Salaita, J. Electron Spectrosc. Rel. Phenom. 134 (2004) 139.
[61] P.R. Norton, G.L. Tapping, J.W. Goodale, Surf. Sci. 65 (1977) 13.